

Dependence of EPSP Efficacy on Synapse Location in Neocortical Pyramidal Neurons

Stephen R. Williams and Greg J. Stuart*

Neurons receive thousands of synaptic inputs throughout elaborate dendritic trees. Here we determine the somatic impact of excitatory postsynaptic potentials (EPSPs) generated at known dendritic sites in neocortical pyramidal neurons. As inputs became more distal, somatic EPSP amplitude decreased, whereas use-dependent depression increased. Despite marked attenuation (>40-fold), when coactivated within a narrow time window (~10 milliseconds), distal EPSPs could directly influence action potential output following dendritic spike generation. These findings reveal that distal EPSPs are ineffective sources of background somatic excitation, but through coincidence detection have a powerful transient signaling role.

Classic views of neuronal operation describe dendrites as funnels, guiding synaptic potentials to the axon where action potential initiation occurs (1). This role is hampered by the filtering effects of the membrane that progressively at-

tenuates and slows the time course of synaptic potentials as they spread from dendritic site of generation to the axon (1, 2). Distal EPSPs are therefore thought to set the background level of somatic depolarization rather than influence the

precise timing of neuronal output (1, 3). Recent evidence, however, indicates that active dendritic mechanisms sculpt the time course of EPSPs in cortical pyramidal neurons to render somatic EPSP time course independent of dendritic site of generation (4, 5). Furthermore, there is evidence that the effects of dendritic filtering on somatic EPSP amplitude in hippocampal pyramidal neurons is overcome by a site-dependent scaling of synaptic conductance (6), as is thought to occur in motoneurons (7). However, controversy over the computational role and universality of site-dependent scaling of synaptic conductance exists (8, 9). Here we examine these issues in neocortical pyramidal neurons.

Pharmacologically isolated spontaneous EPSPs (sEPSPs) were simultaneously recorded at the soma and two apical dendritic sites from layer 5 neocortical pyramidal neurons (Fig. 1A)

Division of Neuroscience, John Curtin School of Medical Research, Australian National University, Canberra, ACT 0200, Australia.

*To whom correspondence should be addressed. E-mail: greg.stuart@anu.edu.au

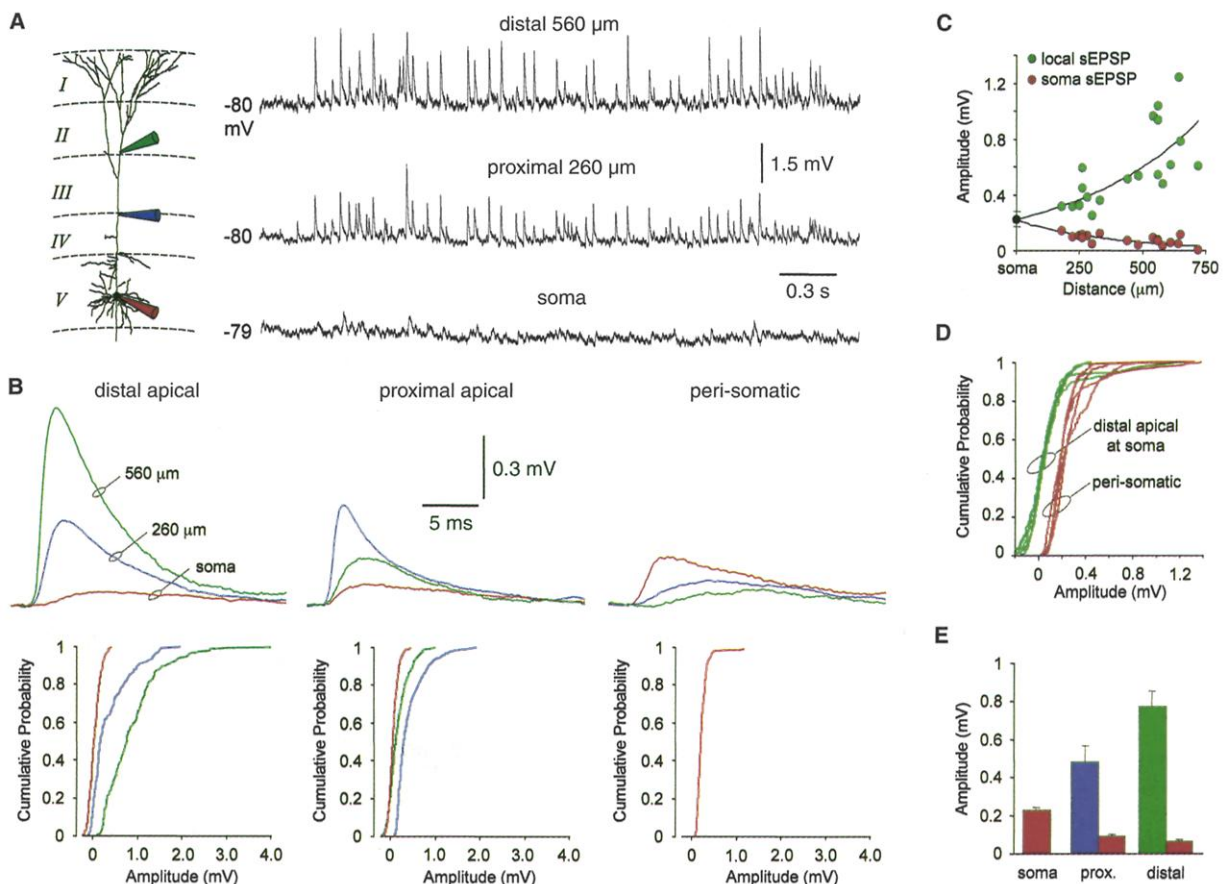


Fig. 1. Site dependence of sEPSP amplitude. (A) Triple recording of sEPSPs at the indicated sites. (B) Averaged sEPSPs (top) and cumulative probability amplitude distributions (bottom) for sEPSPs generated near the indicated sites. (C) Average amplitude of local sEPSPs (green) and the somatic amplitude of these sEPSPs (red) versus the site of sEPSP generation. The average amplitude of perisomatic sEPSPs (\pm SD) is indicated (black). Lines are unconstrained exponential fits. (D) Examples ($n = 5$) of cumulative probability distributions of

somatic sEPSP amplitude for sEPSPs generated at perisomatic (red) and distal apical dendritic (green) sites. Negative amplitude values of small sEPSPs are a product of noise measurement. (E) Red bars show the average amplitude of somatic sEPSPs generated at perisomatic (soma), proximal apical (proximal $284 \pm 25 \mu\text{m}$) and distal apical (distal $590 \pm 24 \mu\text{m}$) sites. The corresponding average amplitude of the local sEPSPs at proximal (blue) and distal apical sites (green) is also shown.

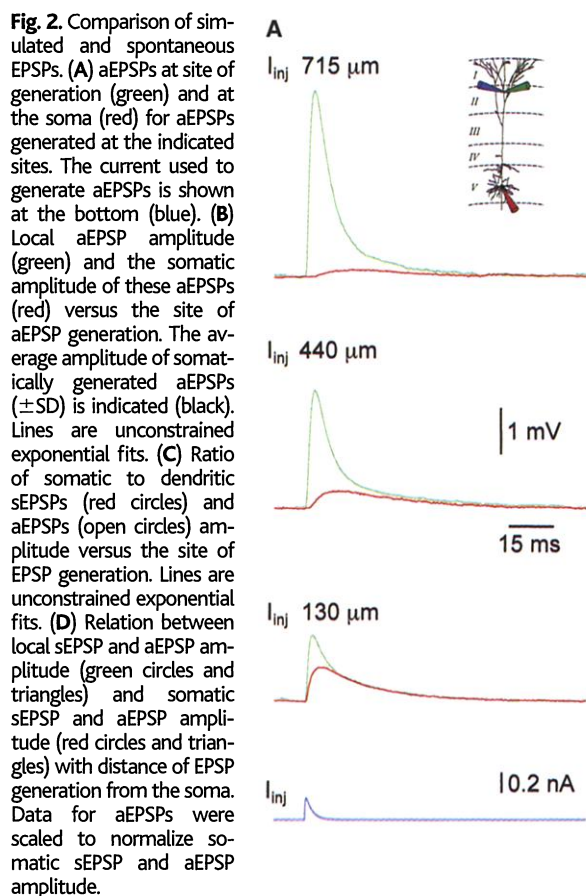
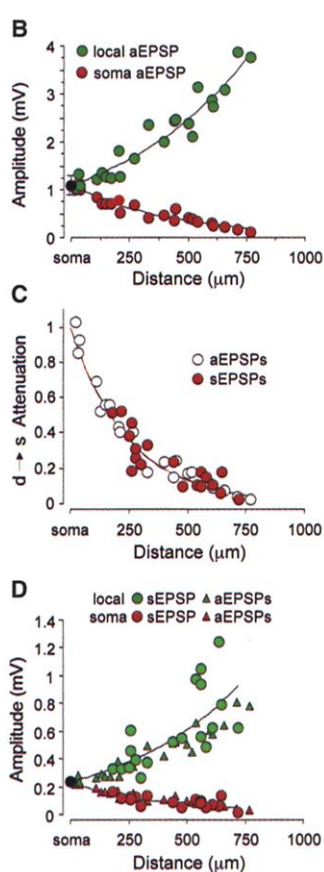
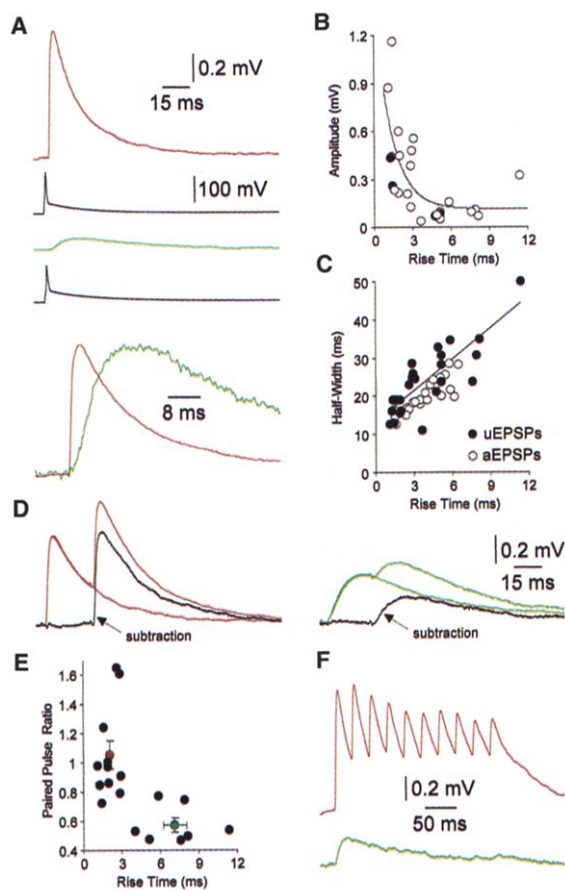


Fig. 2. Comparison of simulated and spontaneous EPSPs. (A) aEPSPs at site of generation (green) and at the soma (red) of aEPSPs generated at the indicated sites. The current used to generate aEPSPs is shown at the bottom (blue). (B) Local aEPSP amplitude (green) and the somatic amplitude of these aEPSPs (red) versus the site of aEPSP generation. The average amplitude of somatically generated aEPSPs (\pm SD) is indicated (black). Lines are unconstrained exponential fits. (C) Ratio of somatic to dendritic sEPSPs (red circles) and aEPSPs (open circles) amplitude versus the site of EPSP generation. Lines are unconstrained exponential fits. (D) Relation between local sEPSP and aEPSP amplitude (green circles and triangles) and somatic sEPSP and aEPSP amplitude (red circles and triangles) with distance of EPSP generation from the soma. Data for aEPSPs were scaled to normalize somatic sEPSP and aEPSP amplitude.

Fig. 3. Site dependence of uEPSPs. (A) Somatically recorded uEPSPs (averages of 100 to 200 trials) following action potentials (black traces) in layer 3 (red) and layer 2 (green) pyramidal neurons. Normalized uEPSPs for comparison of kinetics (bottom). (B) Pooled data demonstrating the exponential (fit to data) relation between uEPSP amplitude and rise time. Filled circles represent neurons in which uEPSPs were also recorded dendritically. (C) Relation between rise time and half-width for uEPSPs (filled circles) and aEPSPs (open circles). The line represents a linear fit to uEPSP data. (D) Dynamic properties of fast (red) and slow (green) uEPSPs. Overlain uEPSPs evoked in response to one and two (25 ms apart) presynaptic action potentials. The black traces are digital subtractions. (E) Relation between the paired-pulse ratio (25 ms) and uEPSP rise time. Colored circles show mean (\pm SEM) values for fast (red, <4-ms rise time) and slow (green, >4-ms rise time) uEPSPs. (F) Fast rising uEPSPs (top) follow action potential trains (40 Hz, 10 action potentials), but slow uEPSPs do not (bottom).



($n = 10$) (10). The hyperpolarization-activated mixed cation conductance, I_h , was blocked to normalize and hyperpolarize the membrane potential throughout the somato-dendritic axis and to remove the effect of I_h on EPSP kinetics (11). sEPSPs were assigned to one of the three recording loci on the basis of their time course and amplitude (Fig. 1B) (12). Selected sEPSPs were largest in amplitude and fastest in time course when recorded closest to their site of generation, and attenuated and slowed as they spread toward other recording sites (Fig. 1B). The local amplitude of sEPSPs increased exponentially (>fourfold) with distance from the soma (Fig. 1C, green circles) (13). Despite this, the somatic amplitude of sEPSPs decreased exponentially as their site of generation became more distal (Fig. 1C, red circles). In all neurons examined, the somatic amplitude of dendritic sEPSPs was significantly smaller ($P < 0.001$) than perisomatically generated sEPSPs (Fig. 1D). On average, the local amplitude of sEPSPs significantly increased ($P < 0.001$) from 0.23 ± 0.02 mV for perisomatically generated events to 0.77 ± 0.08 mV for distal dendritic-generated sEPSPs (Fig. 1E), whereas the somatic amplitude of distal dendritic sEPSPs significantly decreased ($P < 0.001$) to 0.065 ± 0.009 mV (Fig. 1E).

We used current injections to generate artificial EPSPs (aEPSPs) with uniform underlying excitatory postsynaptic current (EPSC) amplitude and kinetics at known dendritic recording sites (14). Double dendritic recording was used to independently inject current and measure aEPSP amplitude at the source (separation between current-injection and voltage-recording electrodes, $9.6 \pm 1.8 \mu\text{m}$; $n = 22$), and somatic aEPSP amplitude was measured with a third pipette (Fig. 2A). The amplitude of dendritic aEPSPs at their site of generation increased exponentially with distance from the soma by up to fourfold (Fig. 2B, green circles), whereas the amplitude of these aEPSPs recorded somatically decreased exponentially with distance (Fig. 2B, red circles). The extent of voltage attenuation from source to soma was similar for aEPSPs and sEPSPs, and could be up to 40-fold at sites more than $750 \mu\text{m}$ from the soma (Fig. 2C). Normalization of data sets at the level of the soma showed a near identical increase in local EPSP amplitude and decrease in somatic EPSP amplitude for aEPSPs and sEPSPs generated at progressively distal dendritic sites (Fig. 2D).

To examine the dependence of somatic EPSP amplitude on synapse location for a homogeneous set of presynaptic inputs, we recorded unitary EPSPs (uEPSPs) between pairs of layer 2/3 and layer 5 neurons (Fig. 3A) ($n = 25$) (15). Across our sample, differences in the somatic time course of uEPSPs were apparent (Fig. 3A). Analysis revealed an exponential decrease in somatic uEPSP amplitude with increasing rise time (Fig. 3B). Because the somat-

ic time course of uEPSPs has been demonstrated to be an accurate predictor of synapse location (16), this finding indicates that the somatic amplitude of uEPSPs declines exponentially as synapse location becomes more distal, as observed for sEPSPs. Our assignment of synapse location on the basis of rise time is further justified by the similar relation between somatic rise time and half-width of uEPSPs and aEPSPs (Fig. 3C) and was independently confirmed during simultaneous somatic and dendritic recording ($n = 4$) (17).

Unexpectedly, we found that the dynamic properties of uEPSPs depended on synapse location (Fig. 3D). Distal uEPSPs exhibited pronounced paired-pulse (25 ms) depression ($42 \pm 5\%$; rise time, 7.1 ± 0.9 ms; $n = 7$), whereas proximal uEPSPs did not exhibit depression ($105 \pm 9\%$; rise time 2.0 ± 0.2 ms; $n = 11$) (Fig. 3E). In response to a train of presynaptic action potentials, proximal synaptic contacts produced a summated series of uEPSPs, whereas distal uEPSPs showed marked depression (Fig. 3F) (18).

The greater than 40-fold dendro-somatic voltage attenuation of distal EPSPs suggests that distal dendritic EPSPs will have little direct impact on neuronal output. Furthermore, the idea that distal dendritic inputs set the background level of somatic depolarization (1, 3) is precluded by the pronounced use-dependent depression of distal EPSPs coupled with the ability of I_h to compensate for the slowing of distal EPSP time course at the soma (4, 5). Because previous findings have revealed the local generation of sodium and calcium spikes in the distal dendrites of pyramidal neurons (19), we hypothesized that distal EPSPs may influence axonal output only through dendritic spike generation (20). To examine this, we generated aEPSPs at distal and somatic sites in the absence of I_h

channel blockers. Dendritic spikes were initiated only when distal aEPSPs were generated coincidentally or slightly (5 ms) offset in time (Fig. 4A) ($n = 15$; average distance from soma of current injection electrode 613 ± 22 μm). Dendritic spikes forward-propagated to the soma (21) and led to the initiation of axonal action potential firing (Fig. 4A) (14 of 15 neurons). The time window for generation of axonal action potentials by distal aEPSPs was narrow (half width, 10 ms; green circles in Fig. 4B) and only slightly increased when aEPSP amplitude was raised by 50% (half width 16 ms) (Fig. 4C). In contrast, generation of somatic aEPSPs with the same underlying aEPSCs produced a significantly broader time window for action potential generation (half-width, 53 ms; red circles in Fig. 4B) (22). The number of action potentials generated by coincident distal dendritic aEPSPs was typically more than generated by somatic aEPSPs (Fig. 4B), indicating that distal excitatory inputs can be more efficacious than somatic inputs. On average, the coincidence of two aEPSPs with a local amplitude of 17.6 ± 1.3 mV (2.3 ± 0.2 mV at the soma; $n = 8$ triple recordings) was required for dendritic spike initiation. Given the large average amplitude of distal dendritic sEPSPs (0.77 mV) and the frequent occurrence of 4 to 10 mV sEPSPs (21), the synchronized activation of between 4 and 30 presynaptic neurons will be required for the initiation of dendritic spikes (23).

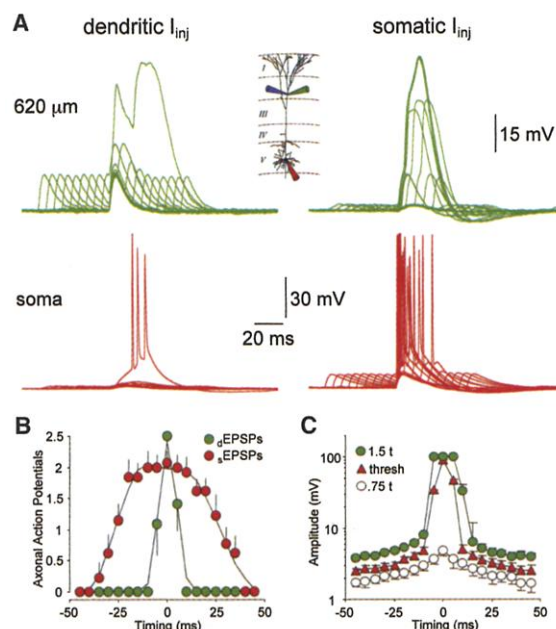
Our findings reveal a uniform synaptic conductance along the apical dendrite of neocortical layer 5 pyramidal neurons, because the distance-dependent increase in local amplitude and dendro-somatic attenuation of sEPSPs was mirrored by aEPSPs generated with a current of uniform amplitude (Fig. 2D). This result is in contrast to that obtained with hippocampal CA1 pyramidal neurons (6) and may be a reflection of the

specialized computational roles played by different classes of neurons. Despite the absence of synaptic scaling, we find a greater than fourfold increase in local dendritic EPSP amplitude at distal dendritic sites. This results from a progressive decrease in input capacitance at more distal dendritic sites and is therefore defined by neuronal geometry, underscoring differences between neuronal types (2, 24, 25). Although the distance-dependent increase in local EPSP amplitude could not compensate for the pronounced electrotonic filtering of the apical dendrite (>40-fold), it enhanced the likelihood that coincident dendritic EPSPs generated dendritic spikes. The narrow time window for local dendritic spike initiation, coupled with the pronounced use-dependent depression of distal EPSPs, suggests that the primary operation of distal dendritic inputs is coincidence detection rather than slow modulation of background somatic depolarization. We anticipate that in vivo compartmentalization of synaptic integration will be further enhanced, because physiological levels of synaptic background activity increase the electrical isolation of distal apical dendrites (9, 26). Functionally, coincidence detection by distal dendritic EPSPs will act to signal synchronized activity in distally located horizontal connections and nonspecific thalamic inputs that convey contextual and attentional relevancy of sensory inputs (27, 28). The pattern of synaptic integration described here may therefore serve to bind at the single-cell level the content and context of sensory information.

References and Notes

1. W. Rall, in *Handbook of Physiology*, vol. 1, *The Nervous System*, E. R. Kandel, Ed. (American Physiological Society, Bethesda, MD, 1977), pp. 39–97.
2. I. Segev, M. London, *Science* **290**, 744 (2000).
3. W. Rall, in *The Theoretical Foundation of Dendritic Function*, I. Segev, J. Rinzel, G. Shepherd, Eds. (MIT Press, Cambridge, MA, 1995), pp. 122–146.
4. J. C. Magee, *Nature Neurosci.* **2**, 508 (1999).
5. S. R. Williams, G. J. Stuart, *J. Neurophysiol.* **83**, 3177 (2000).
6. J. C. Magee, E. P. Cook, *Nature Neurosci.* **3**, 895 (2000).
7. R. Ianssek, S. J. Redman, *J. Physiol. (London)* **234**, 665 (1973).
8. J. C. Magee, *Nature Rev. Neurosci.* **1**, 181 (2000).
9. M. London, I. Segev, *Nature Neurosci.* **4**, 853 (2001).
10. Recordings were made from layer 5 pyramidal neurons in neocortical brain slices (300 μm) prepared from Wistar rats (3 to 5 weeks old) (29), according to methods approved by the Australian National University. Slices were perfused with a solution of composition (mM) 125 NaCl, 25 NaHCO_3 , 3 KCl, 1.25 NaH_2PO_4 , 2 CaCl_2 , 1 MgCl_2 , 3 Na pyruvic acid, 0.1 bicuculline methiodide, and 25 glucose at 35° to 36°C . Simultaneous somatic (pipettes, 2 to 5 megohm; access resistance, <15 megohm) and dendritic (pipettes, 8 to 12 megohm; access resistance, <30 megohm) whole-cell recordings were made with three current-clamp amplifiers. Pipettes were filled with (mM) 135 K-gluconate, 7 NaCl, 10 Hepes, 2 $\text{Na}_2\text{-ATP}$ 0.3 $\text{Na}_2\text{-GTP}$, and 2 MgCl_2 (pH 7.2; KOH). Signals were filtered at 10 kHz and acquired at 30 to 50 kHz. Numerical values are given as the mean \pm SEM. Statistical analysis included Kolmogorov-Smirnov, analysis of variance, and Student's t test.
11. All experiments, except those in Fig. 4, were conducted in the presence of ZD7288 (20 to 50 μM). The membrane potential was -83.4 ± 0.7 mV at somatic and -82.8 ± 0.8 mV at dendritic sites ($n = 10$).

Fig. 4. Time window for synaptic integration depends on synapse location. (A) Summation of aEPSPs generated at distal dendritic (left) and somatic (right) sites in response to pairs of identical aEPSPs separated in time by 0 to 45 ms. Dendritic aEPSPs evoke action potential firing only when activated simultaneously. (B) Average (\pm SEM; $n = 14$) number of somatic action potentials initiated by dendritic (green) and somatic (red) aEPSPs separated by different times. Lines are Gaussian fits. (C) Somatic amplitude of the response to dendritic aEPSPs of different amplitude (0.75 times threshold, open circles; threshold, red triangles; and 1.5 times threshold, green circles). Threshold is defined as the aEPSP amplitude required for dendritic spike generation during coincident activation.



Parallel Single-Cell Monitoring of Receptor-Triggered Membrane Translocation of a Calcium-Sensing Protein Module

Mary N. Teruel and Tobias Meyer*

Time courses of translocation of fluorescently conjugated proteins to the plasma membrane were simultaneously measured in thousands of individual rat basophilic leukemia cells. We found that the C2 domain—a calcium-sensing, lipid-binding protein module that is an essential regulator of protein kinase C and numerous other proteins—targeted proteins to the plasma membrane transiently if calcium was released from internal stores, and persistently in response to entry of extracellular calcium across the plasma membrane. The C2 domain translocation time courses of stimulated cells clustered into only two primary modes. Hence, the reversible recruitment of families of signaling proteins from one cellular compartment to another is a rapid bifurcation mechanism for inducing discrete states of cellular signaling networks.

Studies of the dynamic behavior of signaling systems require the measurement of signaling time courses in individual living cells, because critical cell-to-cell differences are lost in averaged bulk cell measurements (1, 2). One of the most prominent dynamic cell signaling events is the receptor-triggered translocation of signaling proteins with SH2 (Src homology 2), PH (pleckstrin homology), C1, C2, and related domains from the cytosol to the plasma membrane (3, 4). In particular, calcium-sensing C2 domains that exist in ki-

nases, lipases, and many other enzymes and regulatory proteins (5, 6) are intriguing examples of translocation domains because they target signaling proteins to lipid membranes in response to ubiquitously triggered Ca^{2+} signals (7, 8).

We developed an imaging technology based on large-area evanescent wave excitation to simultaneously measure the plasma membrane translocation of the C2 domain from protein kinase C γ (PKC γ) fused to yellow fluorescent protein (YFP) [YFP-C2 domain] (9) in thousands of living rat basophilic leukemia (RBL) cells. In this evanescent wave single-cell array technology (E-SCAT; Fig. 1, A and B) [Web table 1 and Web fig. 1 (10)], cells are grown on a thin glass plate that serves as a uniform guide for laser light with an evanescent field that

12. sEPSPs were detected separately at each recording site with the use of a sliding template algorithm (30) following digital filtering (2 kHz) and displayed together with the voltage response recorded simultaneously at the other recording sites on a fast time base. sEPSPs were accepted as being generated near a recording site if they were fastest rising at that site and had a rise time of less than 3 ms. Experiments with aEPSPs demonstrated that the local amplitude of dendritic EPSPs increased as they were generated more distally. Consequently, at dendritic sites, our procedures detected events generated by EPSCs that would be undetectable if generated at perisomatic sites. To correct for this finding, the threshold amplitude for sEPSP detection was increased for dendritic recording sites on the basis of the experimentally observed increase in local aEPSP amplitude (a procedure that would increase the chance of observing synaptic scaling). The efficacy of event detection was verified by detection of all unitary EPSPs during paired recordings. EPSP rise time represents 10 to 90%, and half-width the duration at half amplitude.
13. The kinetics of dendritic sEPSPs were unrelated to amplitude at each recording site [see (27)].
14. aEPSPs were generated with exponentially rising (0.2 ms) and decaying (2 ms) waveforms of 200-pA amplitude. Kinetics were based on published estimates (37) and reproduced the time course of dendritically generated EPSPs (sEPSPs: rise time 1.11 ± 0.05 ms, half-width 5.97 ± 0.30 ms; aEPSPs: rise time 1.29 ± 0.08 ms, half-width 6.75 ± 0.26 ms).
15. Neurons were morphologically identified following visualization of neurobiotin (0.5 to 2% in pipette solution) staining with standard procedures. We were unable to directly visualize the site of putative contacts made by layer 2/3 pyramidal neuron axons. Single uEPSPs were evoked every 3 s; during paired-pulse experiments uEPSPs were evoked every 5 s, and during action potential trains every 10 s.
16. S. Redman, B. Walmsley, *J. Physiol. (London)* **343**, 117 (1983).
17. uEPSPs with fast somatic kinetics were of smaller amplitude and slower at dendritic recording sites, whereas slow somatic uEPSPs were larger and had faster kinetics at dendritic recording sites.
18. These findings cannot be accounted for by changes in local driving force because during repetitive activation at 40 Hz, each distal dendritic uEPSPs would be expected to have decayed close to baseline before generation of subsequent EPSPs (see Figs. 1B, 2A, and 4A).
19. M. Hausser, N. Spruston, G. J. Stuart, *Science* **290**, 739 (2000).
20. G. M. Shepherd, et al., *Proc. Natl. Acad. Sci. U.S.A.* **82**, 2192 (1985).
21. Supplementary Web material is available on Science Online at www.sciencemag.org/cgi/content/full/295/5561/1907/DC1.
22. The different time window for integration of dendritic and somatic EPSPs results from contrasting local EPSP time courses (dendrite: 6.8 ± 0.3 ms half-width; soma: 18.0 ± 0.9 ms). The longer duration of somatic aEPSPs is a product of neuronal geometry and recruitment of perisomatic noninactivating sodium channels (32, 33).
23. Local EPSP amplitude will be greatest in the apical tuft of layer 5 pyramidal neurons, where initiation of dendritic spikes will be most efficacious (34), reducing the number of coincident EPSPs required for dendritic spike initiation.
24. D. B. Jaffe, N. T. Carnevale, *J. Neurophysiol.* **82**, 3268 (1999).
25. S. J. Redman, *J. Physiol. (London)* **234**, 637 (1973).
26. O. Bernander, R. J. Douglas, K. A. C. Martin, C. Koch, *Proc. Natl. Acad. Sci. U.S.A.* **88**, 11569 (1991).
27. R. Llinas, U. Ribary, D. Contreras, C. Pedroarena, *Philos. Trans. R. Soc. London B Biol. Sci.* **353**, 1841 (1998).
28. C. D. Gilbert, *Neuron* **9**, 1 (1992).
29. S. R. Williams, G. J. Stuart, *J. Physiol. (London)* **521**, 467 (1999).
30. J. D. Clements, J. M. Bekkers, *Biophys. J.* **73**, 220 (1997).
31. M. Hausser, A. Roth, *J. Neurosci.* **17**, 7606 (1997).
32. C. Koch, M. Rapp, I. Segev, *Cereb. Cortex* **6**, 93 (1996).
33. G. Stuart, B. Sakmann, *Neuron* **15**, 1065 (1995).
34. See P. A. Rhodes, R. R. Llinas, *J. Physiol. (London)* **536**, 167 (2001).
35. We thank A. T. Gullledge and B. M. Kampa for helpful discussions. Supported by the Wellcome Trust.

9 November 2001; accepted 15 January 2002

Department of Molecular Pharmacology, Stanford University Medical School, 269 Campus Drive, Stanford, CA 94305, USA.

*To whom correspondence should be addressed. E-mail: tobiasmeyer@stanford.edu

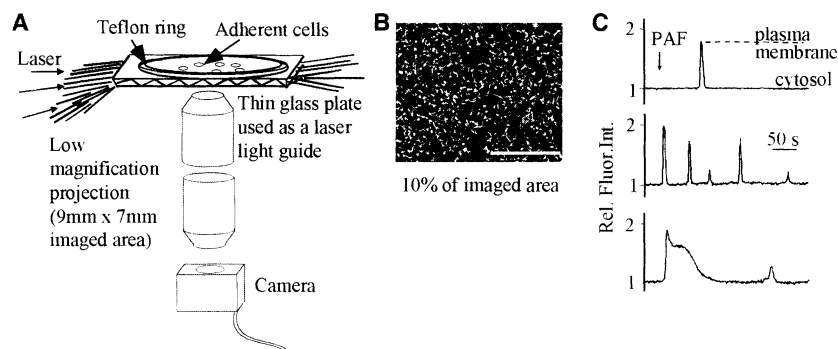


Fig. 1. Simultaneous measurement of plasma membrane translocation events in thousands of individual cells. (A) Schematic view of the E-SCAT system. In this method, an evanescent field is generated above a large surface area by coupling a laser into the angled edge (15°) of a glass plate 200 μ m thick (10, 29). A high numerical aperture projection system was built to image a 7 mm by 9 mm region at the glass-water interface onto a CCD camera (30). Up to \sim 100,000 cells can be plated in this region. (B) A 10% subregion of an E-SCAT image used for translocation time course analysis [full image shown in Web fig. 3 (10)]. Each bright spot reflects a transfected RBL cell whose surface plasma membrane is excited by evanescent wave excitation. Scale bar, 1 mm. (C) Representative time courses of relative fluorescence intensity reflecting three single-cell translocation events in RBL cells transfected with YFP-C2 domain after addition of a submaximal concentration of PAF (final concentration 1 nM).